Zero-Flux Surfaces of the Electrostatic Potential: The Border of Influence Zones of Nucleophilic and Electrophilic Sites in Crystalline Environment

Ignasi Mata,[†] Elies Molins,[†] and Enrique Espinosa*[,‡]

Institut de Ciència de Materials de Barcelona (ICMAB-CSIC), Campus UAB, 08193 Bellaterra, Spain, and Laboratoire de Cristallographie et Modélisation des Matériaux Minéraux et Biologiques, LCM³B, UMR CNRS 7036, Faculté des Sciences Université Henri Poincaré− Nancy 1, BP 239, 54506 Vandoeuvre-lès-Nancy, France

Received: May 24, 2007; In Final Form: July 10, 2007

The topology of the electrostatic potential $\varphi(\mathbf{r})$ has been studied for single molecules using geometries and electron distributions $\rho(\mathbf{r})$ determined from high-resolution single-crystal X-ray diffraction data. The electrostatic potential gradient $\nabla\varphi(\mathbf{r})$, which is the negative of the electric field $\mathbf{E} = -\nabla\varphi$, has been represented, revealing the position of zero-flux surfaces and critical points. Local maxima and minima of the electrostatic potential are interpreted in terms of electrophilic and nucleophilic sites, which present influence zones delimited by zero-flux surfaces containing saddle points. The influence zones of the nucleophilic and electrophilic sites define two alternative partitions of the space in disjoint volumes, the completeness of these partitions depending on either the neutral or ionic character of the molecule. The results obtained by using this methodology are useful for the interpretation of the saddle points of the electrostatic potential, which are related to the limits of the influence zones and reveal the path for preferred attack on reactive sites with finite influence zones.

1. Introduction

The molecular electrostatic potential[1,2] $\varphi(\mathbf{r})$ is extensively used in the analysis of the molecular reactivity, as it allows the identification of the nucleophilic and electrophilic regions of the molecule. The topological analysis of $\varphi(\mathbf{r})$ has been developed in order to exploit the information contained on this scalar field, following a procedure similar to that developed for the electron density distribution $\rho(\mathbf{r})$ on the framework of the Atoms in Molecules (AIM) theory,[3] which has been successfully applied to the study of many types of interatomic interactions.

Topological analysis of a scalar field as $\rho(\mathbf{r})$ or $\varphi(\mathbf{r})$ relies on the calculation of its gradient, from which features such as the critical points, which are associated to local extrema and to saddle points, can be found. In the analysis of $\rho(\mathbf{r})$, all these points are associated to chemical concepts such as bonds or rings, whereas in the electrostatic potential $\varphi(\mathbf{r})$ an interpretation has been provided only in some cases. For example, local minima are related to local concentrations of electrons, such as lone pairs or double bonds, and saddle points between covalently bonded atoms define an equivalent to the bond critical point of $\rho(\mathbf{r})$ in the $\varphi(\mathbf{r})$ topology.[4] Further interpretation is obtained from the correlation of the position of the critical point or the values of local properties on it with properties of the system. Thus, the position of the local minima associated to lone pairs and the value of $\varphi(\mathbf{r})$ at this point has been related to the strength of hydrogen bonds,[5,6] and the position of the $\varphi(\mathbf{r})$ bond critical point has been used to determine the relative electronegativities and the radii of atoms.[7−9] The interpretation of the topological properties has been much more elaborated for $\rho(\mathbf{r})$ than for $\varphi(\mathbf{r})$ due to the development of the AIM theory for the former. Moreover, $\varphi(\mathbf{r})$ on molecules presents a large diversity of critical points outside the bonding regions,[10,11] most of them without a clear interpretation, a feature not observed in the topology of $\rho(\mathbf{r})$.

The zero-flux surfaces S of a scalar field $\zeta(\mathbf{r})$ are defined as the set of points $\mathbf{r}$ holding

$$\nabla\zeta(\mathbf{r})\cdot\mathbf{n}(\mathbf{r}) = 0, \quad \forall\mathbf{r} \in S \tag{1}$$

where $\mathbf{n}(\mathbf{r})$ is the unit vector perpendicular to S at $\mathbf{r}$. Again, the interpretation of zero-flux surfaces is far less elaborated for $\varphi(\mathbf{r})$ than for $\rho(\mathbf{r})$, for which they correspond to a quantum mechanics-based partition of the space, leading to the atomic volumes. In the analysis of $\varphi(\mathbf{r})$, zero-flux surfaces are also observed between atoms,[12,13] but the actual partition of the space in volumes is different from that of the electron density. Characteristic of $\varphi(\mathbf{r})$ is also the surface completely enclosing the molecule when it presents a negative charge.[14] This kind of surface has been proposed as the molecular border in the case of anions.[15]

In order to deepen in the interpretation of the critical points and zero-flux surfaces of $\varphi(\mathbf{r})$, the gradient of this quantity has been represented for several molecules and ions. This has permitted the visualization of these topological features and has enable exploration of both the relationships between them and their implication in the molecular electrostatic interaction. Most of the analysis has been performed by comparison with the well-known topology of the electron density, an approach yet used for the analysis of the electrostatic potential.[4] Both the electrostatic potential and its gradient, which is the negative of the electric field, are physical observables that can be determined by high-resolution X-ray diffraction.[16] This can be done by fitting these quantities against the experimental structure factors, or, more commonly, via the experimental electron density, previously obtained by a fit against the same structure factors.[17]

As we are mainly interested in the analysis of the molecular electrostatic potential, this work deals with pseudo-isolated

* Corresponding author. E-mail: enrique.espinosa@lcm3b.uhp-nancy.fr.
† Institut de Ciencia de Materials de Barcelona.
‡ Faculté des Sciences Université Henri Poincaré.

10.1021/jp074032l CCC: $37.00
Published on Web 08/30/2007

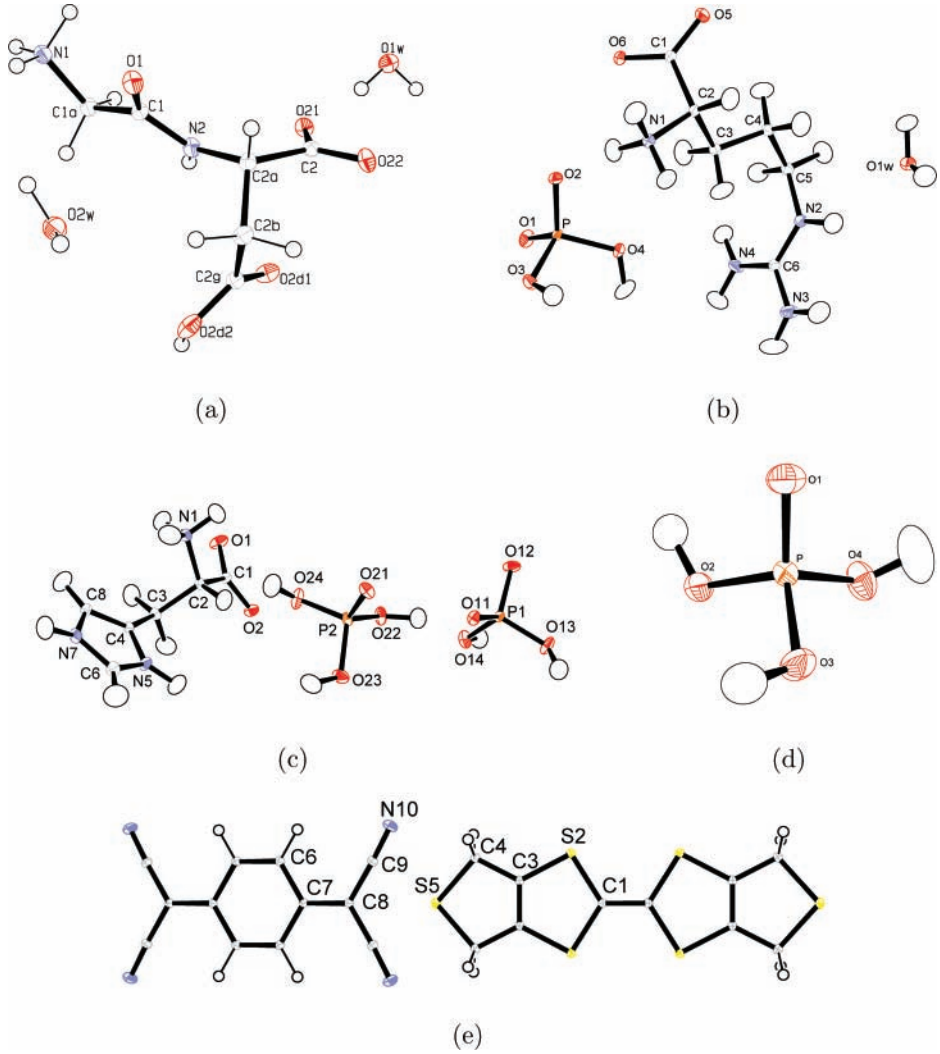

Figure 1. ORTEP views of the molecular units of (a) GD, (b) LAP, (c) LHP, (d) phosphoric acid, and (e) BTDMTTF−TCNQ.

molecules (i.e., single molecules exhibiting the same electron density distribution as observed in the crystal). The studied systems have been taken from several previously published electron density studies: the glycyl-aspartic acid dihydrate (GD),[18] the L-argininium phosphate monohydrate (LAP),[19] the L-histidinium phosphate phosphoric acid (LHP),[20] the phosphoric acid,[21] and the bis(thiodimethylene)−tetrathiafulvalene tetracyanoquinodimethane (BTDMTTF−TCNQ).[22] The ORTEP views[23] of the molecular units of these crystals are shown in Figure 1.

2. Methodology

All the electron distributions used for the calculation of $\varphi(\mathbf{r})$ and its gradient were defined in terms of the Hansen−Coppens multipolar model,[24] where the total electron density is given by the superposition of atomic densities, each of them represented by a multipolar expansion centered at the atomic position:

$$\rho_{at}(\mathbf{r}) = \rho_{core}(r) + P_v\kappa^3\rho_{val}(\kappa r) + \sum_{l=0}^{l_{max}}\sum_{m=0}^{l}\kappa'^3 R_{nl}(\kappa' r)\, P_{lm\pm} y_{lm\pm}(\theta,\varphi) \quad (2)$$

where $\rho_{core}(r)$ and $\rho_{val}(r)$ respectively represent the free atom core- and the valence-shell electron density distributions. $R_{nl}(r)$ is a Slater-type radial function, and $y_{lm\pm}(\theta,\varphi)$ are spherical harmonic functions in real form. P_v and $P_{lm\pm}$ are the multipolar population parameters, and κ and κ' are expansion/contraction coefficients. Similar expansions for $\varphi(\mathbf{r})$ and for the components of its gradient can be obtained from the terms of the multipolar expansions obtained for the atomic densities.[25]

As the topological analysis of the electrostatic potential is not available in the common software used for the analysis of the experimental electron density, a new program was developed for the calculation of the $\varphi(\mathbf{r})$ gradient by modifying a self-developed program for the topological analysis of the experimental electron density, completely written by ourselves in programming language *C*. The quality of our code was tested by comparing $\varphi(\mathbf{r})$ and the topology of $\rho(\mathbf{r})$ calculated from our program with the results obtained from other softwares.[26,27]

In the following figures, bidimensional representations of the gradient, are obtained by projecting the gradient vector on the represented plane. Gradient lines obtained in this way do not correspond to the tridimensional field, but provide a well-adapted visualization of the intersection of the zero-flux surfaces with the plane, appearing as lines not crossed by any field line. The projections of the critical points on the planes appear as points where gradient lines converge or diverge. In the bidimensional maps, local extrema appear always as points where the gradient lines converge, while for saddle points both behaviors can be observed, depending on the chosen plane. Moreover, critical points that are far from the planes are

projected on them, thus making the interpretation more difficult. In some cases, a representation of the scalar field or its gradient on a perpendicular plane is useful for the characterization of a particular point.

3. Results and Discussion

3.1. The Critical Points of the Electrostatic Potential. The topological analysis of any scalar field is based on the application of the gradient and Laplacian to this field. In the case of the electrostatic potential, these operators have a clear physical significance: $\nabla\varphi(\mathbf{r})$ is the negative of the electric field, while $\nabla^2\varphi(\mathbf{r})$ is related to the charge density by Poisson's equation:

$$\nabla^2\varphi(\mathbf{r}) = 4\pi(\rho(\mathbf{r}) - \sum_j Z_j\delta(\mathbf{r} - \mathbf{R}_j)) \quad (3)$$

where Z_j and R_j are respectively the atomic number and the position of the j-nucleus and $\delta(\mathbf{r})$ is the Dirac delta.

The electric field shows the position of the critical points, as these are the points holding the equation:

$$\nabla\varphi(\mathbf{r}) = 0 \quad (4)$$

The eigenvalues of the Hessian matrix at these points are the curvatures of the electrostatic potential. According to Poisson's equation and to the condition $\rho(\mathbf{r}) > 0$, the sum of the curvatures must be positive outside the nuclear positions. Critical points are classified according to a pair of numbers (R, S) derived from the curvatures: the rank R is the number of nonzero curvatures, while the signature S is the algebraic sum of the signs of the curvatures.

The most common critical points in $\varphi(\mathbf{r})$ and $\rho(\mathbf{r})$ have $R = 3$. Nevertheless, in some special cases, points with $R < 3$, known as degenerate critical points, can arise. While in $\rho(\mathbf{r})$ degenerate points only appear outside the equilibrium geometry and are associated to situations of structural instability,[28] in the case of $\varphi(\mathbf{r})$ they can appear in the ground state if the system presents cylindrical or spherical symmetry.[29] As this is not the case of the experimental cases studied here, only nondegenerate critical points will be considered.

According to its signature, rank 3 critical points can be classified as four types: (3, −3), (3, −1), (3, +1), and (3, +3). First and last types correspond to local maxima and minima, respectively, while second and third types are saddle points.

Local maxima of $\varphi(\mathbf{r})$ can only happen at nuclear positions, as these are the unique points where the sum of the curvatures is not necessarily positive.[14,30] If nuclei are treated as punctual particles, $\varphi(\mathbf{r})$ tends toward infinity at their positions, and therefore it must be noticed that curvatures are not defined at the local maxima. Accordingly, the condition of local maxima of $\varphi(\mathbf{r})$ at the atomic nuclei is not revealed by the Hessian matrix of $\varphi(\mathbf{r})$ but by its behavior in the surroundings of the nuclear positions.

Local minima of $\varphi(\mathbf{r})$ are related to local concentrations of the electron density, such as those observed in lone pairs or in double and triple bonds. These local minima are often situated in the surroundings of the molecule, a feature not observed in the case of $\rho(\mathbf{r})$. In general, they are associated to regions of negative $\varphi(\mathbf{r})$, giving rise to an asymptotic behavior different from that of $\rho(\mathbf{r})$ as the distance to the molecule increases. Thus, while $\rho(\mathbf{r})$ always tends asymptotically to zero from positive values, $\varphi(\mathbf{r})$ can go asymptotically to zero from positive or negative values.

The more complex asymptotic behavior of $\varphi(\mathbf{r})$ requires a more general form of the Poincaré−Hopf relationship, which relates the number of the four types of critical points. For $\varphi(\mathbf{r})$, this relationship is:[10]

$$n_{-3} - n_{-1} + n_{+1} - n_{+3} = n_+ - n_- \quad (5)$$

where n_S is the number of critical points with signature S, and n_+ and n_- stand for the number of asymptotic maxima and minima. The latter correspond to the regions of solid angle where $\varphi(\mathbf{r})$ is going asymptotically to zero from positive and negative values, respectively. The Poincaré−Hopf relationship for $\rho(\mathbf{r})$ corresponds to the particular case $n_+ = 1$ and $n_- = 0$.

3.2. Space Partition from the Electric Field. As seen in the topological analysis of $\rho(\mathbf{r})$, most of the $\varphi(\mathbf{r})$ gradient lines start and end at critical points, the rest having one of their extremes at infinity. The set of gradient lines $\nabla\rho(\mathbf{r})$ starting at a nuclear position, which corresponds to a tridimensional attractor of $\rho(\mathbf{r})$ and therefore to a (3, −3) critical point, defines a volume limited by a zero-flux surface S_ρ associated to the atom.[31] Atomic volumes are thus called atomic basins (ρ-basins). Other kind of basins (φ-basins) are obtained from $\varphi(\mathbf{r})$. In this case, they correspond to the volumes covered by the sets of electric field lines starting at the same nuclear positions and limited by zero-flux surfaces S_φ. Thus, the boundaries of the ρ- and φ-basins are the zero-flux surfaces S_ρ and S_φ, which hold eq 1 and are not crossed by any gradient field line.

The shape and size of the φ- and ρ-basins are very different. For example, negatively charged atoms exhibit φ-basins completely enclosed by zero-flux surfaces, even if they are situated in the periphery of the pseudo-isolated molecule, a feature not observed for the ρ-basins.[13] An example is shown in Figure 2 for one of the cocrystallized water molecules in the crystal structure of GD. The three ρ-basins expand outside the molecule and formally have infinite volume, in spite of the fact that this is not clear in Figure 2b. Indeed, the electron density distributions of pseudo-isolated molecules that are parametrized with multipolar models present artifacts far from the nuclear positions, mainly associated to the extension of the radial functions in regions where $\rho(\mathbf{r}) \simeq 0$ or where the contributions of neighboring molecules in the crystal can be significant, therefore leading to an artificial border of the atomic basin. This problem does not exist for $\varphi(\mathbf{r})$ as this is a long-range property that decays much more slowly with the distance to the nuclei, thus being still significant in regions where $\rho(\mathbf{r})$ falls within variance values. As seen in Figure 2a, the φ-basin of the oxygen is completely enclosed by a zero-flux surface, while the space outside the molecule is filled by the φ-basins of the hydrogens. According to the Gauss theorem, the net charge in basins completely surrounded by zero-flux surfaces must be zero. Thus, any φ-basin with finite volume is neutral, and if the atom is negatively charged, the excess of electron density falls outside its φ-basin, as shown for nitrogen atoms in a recent theoretical study of the electrostatic potential involving N···H hydrogen bonds.[32]

In Figure 2, the electric field lines inside the φ-basins of the hydrogen atoms end at the electrostatic potential minima in the surface of the oxygen φ-basin. In the case of neutral molecules, the total flux of electric field that crosses a hypothetical surface containing all the charge of the molecule must be zero. This surface is formally placed at infinity, and the flux is zero on all its points. Another hypothetical surface, situated at a finite distance but enclosing all the critical points of the molecule, would present regions of positive flux (from the molecule) and negative flux (to the molecule) of the electric field, correspond-

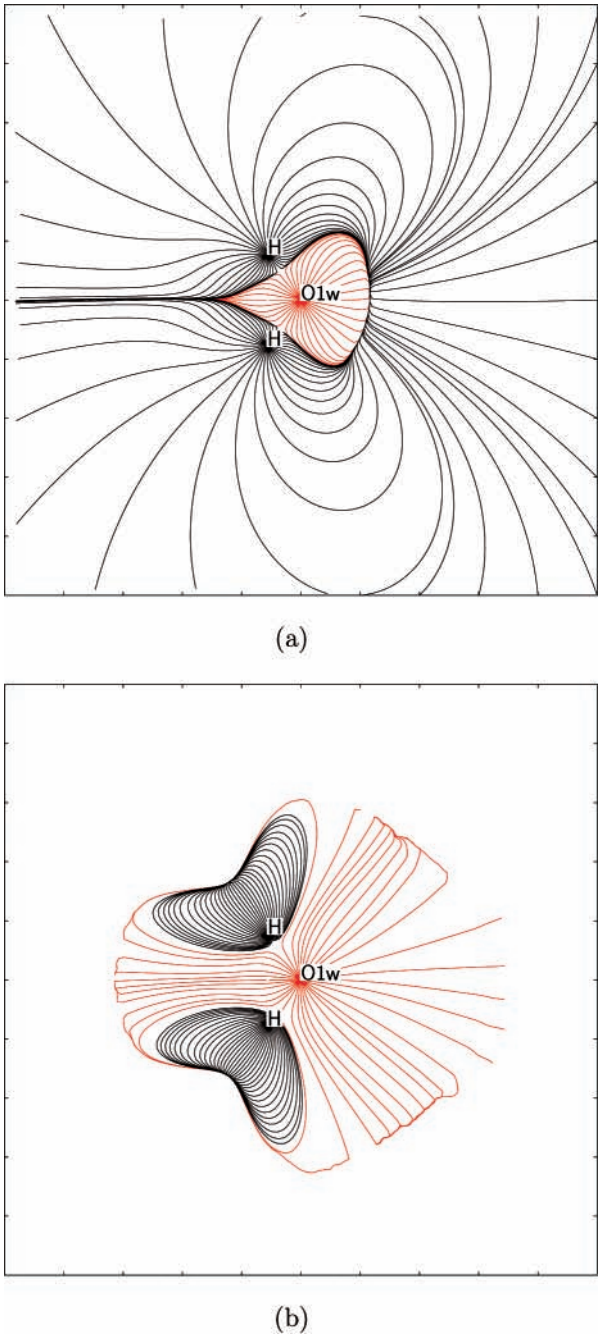

Figure 2. Experimental gradient lines of (a) $\varphi(\mathbf{r})$ and (b) $\rho(\mathbf{r})$ calculated in the plane of one of the cocrystallized water molecules in the crystal structure of GD (Figure 1a). Red and black lines are used for the basins of oxygen and hydrogen atoms, respectively. Ticks are set at each 1 Å.

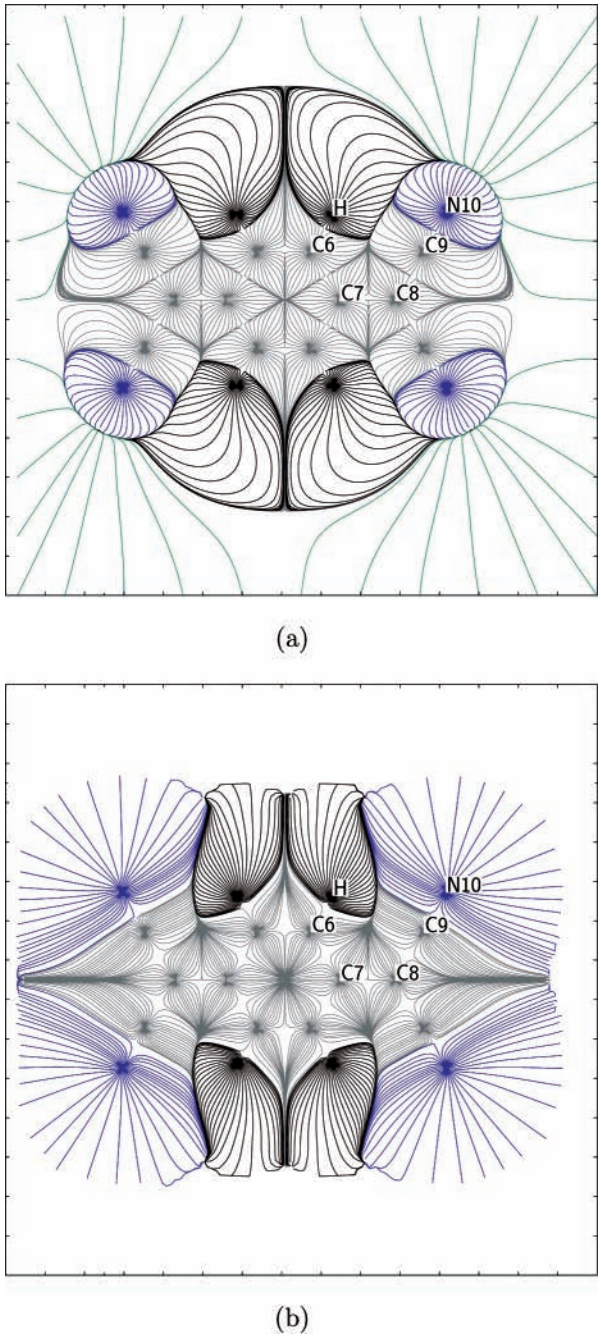

Figure 3. Experimental gradient lines of (a) $\varphi(\mathbf{r})$ and (b) $\rho(\mathbf{r})$ in the plane of the TCNQ anion of the BTDMTTF−TCNQ complex (Figure 1e). Gray, blue and black lines are used for the basins of the C-, N-, and H-atoms, respectively. Green lines are used for the volume not belonging to any nuclear φ-basin. Ticks are set at each 1 Å.

ing to the asymptotic maxima and minima of the electric field.[10] This last surface should exhibit an almost zero net flux and therefore enclose a region with approximately zero net charge. Thus, electric field lines starting at the nuclear positions cross the surface outward in regions of positive flux, then describe loops that cross it again inward in regions of negative flux, and end at the local minima of the molecule. The electric field lines starting on the nuclei belonging to a neutral molecule fill all the space. Thus, the partition in φ-basins is complete, and the zero net charge of the neutral molecule is obtained by addition of the contributions of these electrostatic regions which are formally limited by the zero-flux surface placed at infinity.

In the case of ions, due to the net charge of the molecule, there is a single asymptotic maximum (anions) or minimum (cations), independent of the local maxima or minima in the surroundings of the molecule (see eq 5). Thus, the total flux of electric field lines that cross all the surface elements enclosing the ion is negative (anions) or positive (cations), respectively. The negative flux in the case of anions implies the existence of electric field lines starting at infinity and ending at the local minima of $\varphi(\mathbf{r})$ in the molecule. The space filled by these field lines does not belong to any φ-basin including a nucleus, thus excluding a complete partition of the space in this kind of φ-basins for the anions, as seen in Figure 3 for the anionic moiety of the charge-transfer complex BTDMTTF−TCNQ.[22] In that case, while the ρ-basins of nitrogen and hydrogen atoms expand outside the molecule and have infinite volume, all the φ-basins including a nucleus have finite volume. As

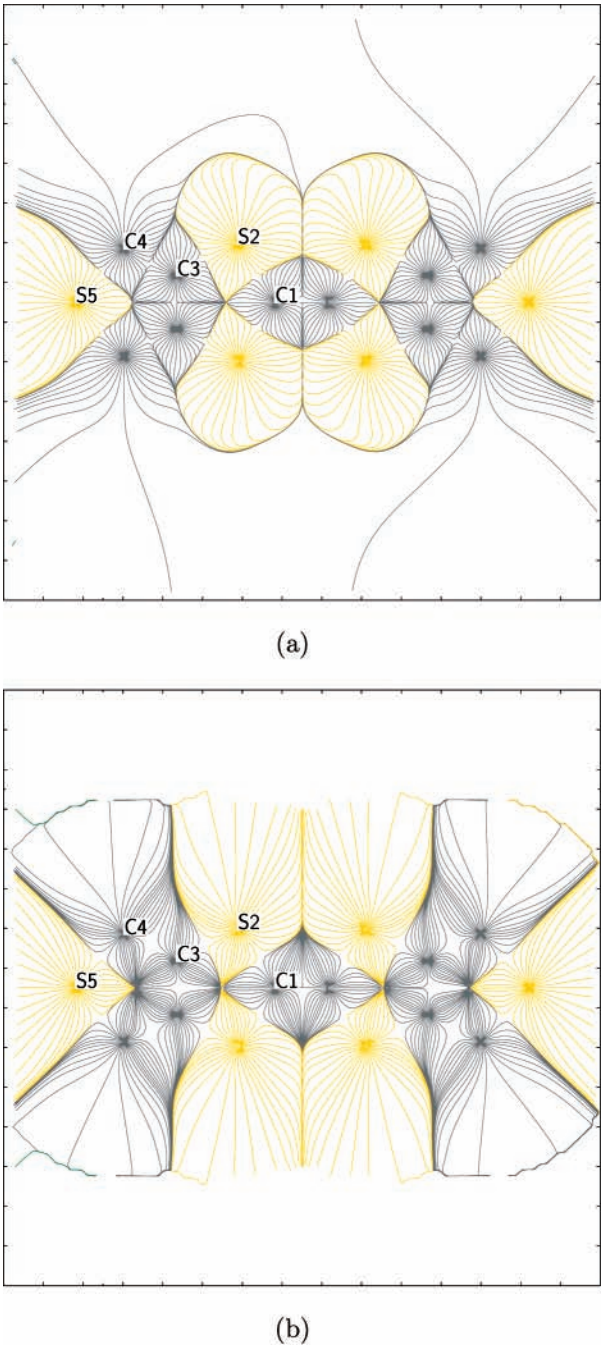

Figure 4. Experimental gradient lines of (a) $\varphi(\mathbf{r})$ and (b) $\rho(\mathbf{r})$ in the plane of the BTDMTTF cation of the BTDMTTF−TCNQ complex (Figure 1e). Gray and yellow colors are used for the basins of the C- and S-atoms, respectively. Ticks are set at each 1 Å.

expected for anions,[15] there is a zero-flux surface enclosing a volume that contains all the nuclei and has zero net charge. Hence, the excess of electron density falls outside this surface, in the region that does not belong to any φ-basin possessing a nucleus.

In the case of cations, the electric field lines crossing the surface (that contains all the positive and negative charges) outwardly start at nuclear positions, and a complete partition of the space in φ-basins possessing a nucleus is found. Contrary to neutral molecules, electric field lines in the surrounding areas of cations do not describe loops to end at local minima, as shown in Figure 4 for the BTDMTTF moiety of the BTDMTTF−TCNQ complex. In spite of finite φ-basins that include a nucleus being observed for the inner part of the cation (namely, the tetrathiafulvalene TTF group), the φ-basins corresponding to the outer thiodimethylene TDM groups fill the space surrounding the molecule. As the finite TTF φ-basins present zero net charge, the extended TDM φ-basins must exhibit a positive net charge. Thus, the electric field lines reveal the parts of the molecule that are positively charged, as the atoms in these regions present infinite φ-basins.

3.3. Nucleophilic and Electrophilic Regions. In the analysis of the electrostatic potential, on one hand negative values of $\varphi(\mathbf{r})$ are associated to nucleophilic regions where an electrophilic attack can be expected. On the other hand, the recognition of electrophilic regions is not straightforward because $\varphi(\mathbf{r})$ is positive everywhere but in the well-localized nucleophilic regions, thus making it difficult to point to the most suitable sites for nucleophilic attacks within the wide region of positive $\varphi(\mathbf{r})$.

This difficulty is avoided by mapping $\varphi(\mathbf{r})$ on surfaces far enough from the nuclei to contain almost all the molecular electron density, as for example on van der Waals surfaces or on isosurfaces of $\rho(\mathbf{r})$ with a small value of this molecular property. Hence, the maxima and minima of $\varphi(\mathbf{r})$ on these surfaces show the position of electrophilic and nucleophilic sites, respectively. The representation of the electric field on similar enclosing surfaces has also been used for the same purpose,[5,33] showing relationships between the magnitude of the electric field on the surface and the reactivity of the molecule.

The electric field lines complement the mapping of $\varphi(\mathbf{r})$ on surfaces by revealing the trajectory of the field lines crossing these surfaces. For example, in parts a and b of Figure 5, the field lines and the electrostatic potential created by the phosphoric acid molecule[21] are represented together with its van der Waals envelope. The minima of $\varphi(\mathbf{r})$ associated to the lone pairs of the oxygens (Figure 5b) are placed at the positions where the field lines converge (Figure 5a) very close to the van der Waals surface. Figure 5a shows the electric field generated around
two hydrogen atoms and two oxygen acceptors involved in hydrogen bonds in the phosphoric acid crystal structure. The corresponding electrophilic and nucleophilic sites are respectively revealed by local maxima and minima of $\varphi(\mathbf{r})$ on the van der Waals surface.

On the same figure, apart from small regions belonging to the φ-basins of P and O3, the electric field lines outside the van der Waals surface have their origin in one of the hydrogen atoms. Thus, the space outside the molecule can be divided into two regions, namely the φ-basins possessing the H-nuclei and corresponding to the influence zones of both electrophilic regions. Thus, a negative probe-charge outside the van der Waals surface would be attracted toward one of the hydrogens, depending on the φ-basin in which it is situated. An analogous partition can be established by using the end point of the field lines instead of their origin, thus dividing the space into two regions, corresponding to the influence zones of the two nucleophilic regions associated to the oxygen lone pairs and separated by a zero-flux surface passing through both H-nuclei (Figure 6a).

This new partition, which is based on the local minima instead of the local maxima, is rarely used in the topological analysis of the electron density. However, it has been applied to the analysis of ionic crystals,[34,35] leading to the development of the concept of *primary bundles*, which are defined as the volumes filled by the set of all gradient lines starting and ending at the same pair of maximum/minimum extrema. A detailed explana-

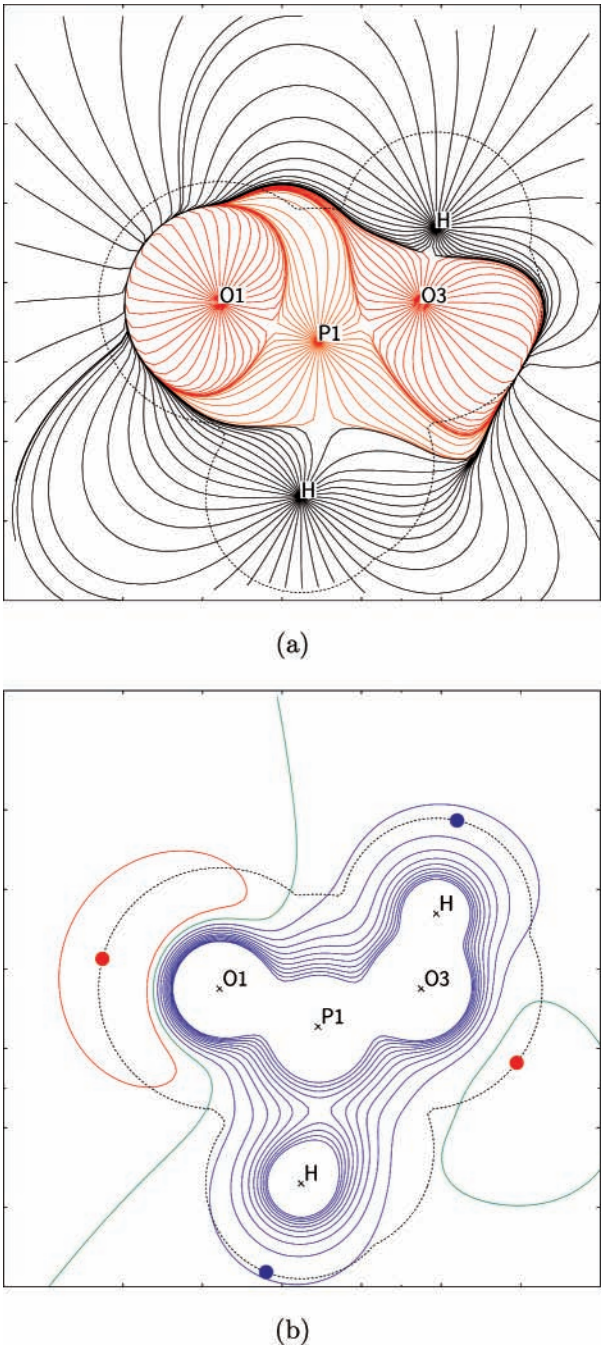

Figure 5. (a) Experimental gradient lines of $\varphi(\mathbf{r})$ and (b) $\varphi(\mathbf{r})$ of the phosphoric acid molecule (Figure 1d). The plane is defined by the atoms O1, O2, and its hydrogen H(O2). In (a), orange, red, and black colors are for the basins of P-, O-, and H-atoms, respectively. Contours in (b) are set at each 0.1 e Å^{-1}. Blue and red contours represent positive and negative values, respectively. The green contour corresponds to the zero value. In both diagrams, the van der Waals surface is represented by a dashed contour. In (b), local maxima and minima on the van der Waals surface are marked with blue and red circles, respectively. Ticks are set at each 1 Å.

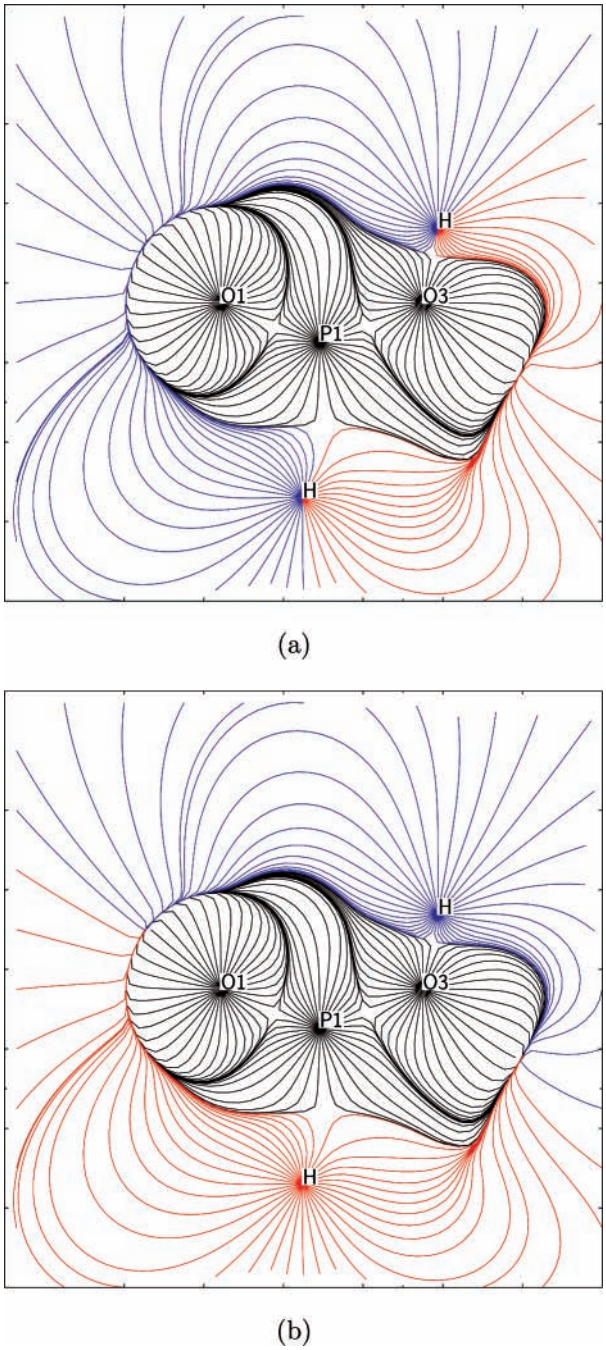

Figure 6. Experimental gradient lines of $\varphi(\mathbf{r})$ in the same plane as in Figure 5. The blue and red lines stand for the two (a) nucleophilic and (b) electrophilic influence zones in the surroundings of the phosphoric acid molecule.

tion of the fundamentals and the properties of primary bundles can be found in refs 34 and 35.

In the topology of the electrostatic potential, the partitions in local maxima and local minima can be combined by supposing that both kinds of influence zones are composed of one or more primary bundles. As bundles are delimited by zero-flux surfaces, their grouping to form nucleophilic (Figure 6a) or electrophilic (Figure 6b) influence zones gives always volumes enclosed by these surfaces. In Figure 5 most of the space outside the van der Waals surface is filled by four primary bundles, which can be alternatively grouped into two local maxima or two local minima basins that correspond to two electrophilic and nucleophilic influence zones, respectively.

In the case of neutral molecules, all the electric field lines start and end on local extrema. Thus, any primary bundle belongs to the influence zones of nucleophilic and electrophilic sites at the same time. A positive probe-charge inside this bundle is pushed away from the electrophilic site and directed toward the nucleophilic one, and the reverse for a negatively charged probe. It must be noticed that, as the electric field lines of the bundle are generated by the charge distribution of the whole

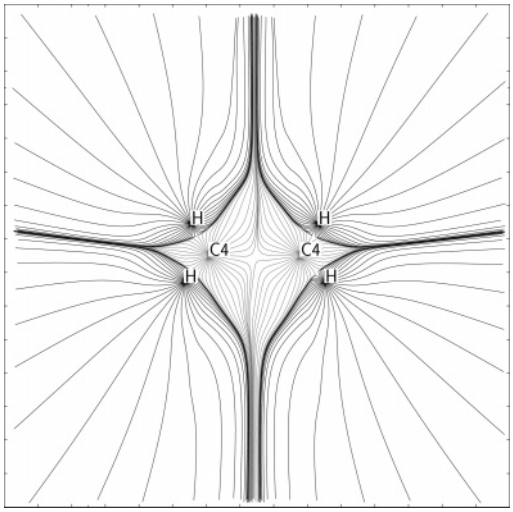

Figure 7. Experimental gradient lines of $\varphi(\mathbf{r})$ in the plane perpendicular to the BTDMTTF cation of Figure 4, containing both carbon atoms of the TDM group. Gray and black colors are used for the basins of C and H, respectively. Ticks are set at each 1 Å.

molecule, it is the interaction of the charge with the molecular charge distribution that pushes the former toward a particular reactivity site at one of the borders of the bundle.

In the case of ions, there are primary bundles with only one extreme on the molecule. These bundles belong to the φ-basins with infinite volume in cations, or they fill the external region outside the molecule in anions. Thus, while for the TCNQ anion (Figure 3) the surroundings of the molecule are divided in four influence zones corresponding to the four nucleophilic sites of the CN groups, for the BTDMTTF cation (Figure 4) the influence zones of the electrophilic sites in the TDM groups expand outward the molecule. Figure 4 suggests that the carbons in the TDM present a large φ-basin that would surround the TTF group. However, the representation of the field in the plane perpendicular to the molecule (Figure 7) shows that the φ-basins associated to these atoms are contracted along this plane, the φ-basins of the hydrogens bonded to the carbon atoms filling most of the volume around the molecule.

Anions and cations can also respectively present electrophilic and nucleophilic functional groups on their surfaces. The influence zones of these groups are limited in the space, as the monopolar moment of the ion must prevail at long distances. Thus, the electric field around the electrophilic carboxyl group in the cation of the LHP crystal structure[20] (Figure 8) clearly shows the influence zone of this functional group limited by a zero-flux surface. In the plane, this zone is formed by two primary bundles starting at two hydrogen atoms and ending at the potential minima close to the oxygen atoms. Outside the influence zone, the field lines bypass the carboxyl group, while inside they converge on the local minima. A positive probe-charge located inside the volume delimited by the zero-flux surface will be attracted toward the functional group of the molecule, whereas if it is standing outside, it will be repelled.

Another example is given in Figure 9, where the field lines around the phosphate group in LHP are represented. In contrast with the phosphoric acid molecule shown in Figure 5, the φ-basin associated to the hydrogen atom that is involved in a hydrogen bond interaction in the LHP crystal structure is finite and surrounded by a zero-flux surface. A negatively charged probe outside this φ-basin is repelled by the negative charge of the anion, while inside it is attracted toward the hydrogen.

Neutral molecules can also present functional groups with finite influence zones, as shown in Figure 10 for the glycyl-

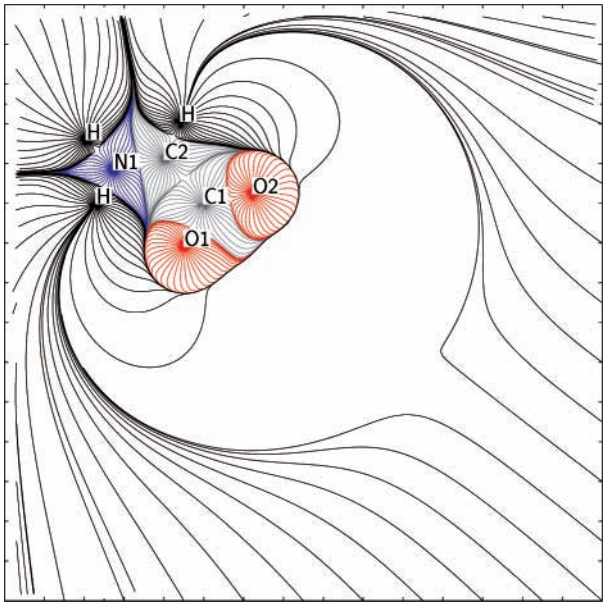

Figure 8. Experimental gradient lines of $\varphi(\mathbf{r})$ in the surroundings of the carboxyl group belonging to the histidinium cation of the LHP (Figure 1c). The plane is defined by C1 and two hydrogens, one bonded to N1 and the other to C2. Red, blue, gray, and black lines stand for basins of O-, N-, C-, and H-atoms, respectively. Ticks are set at each 1 Å.

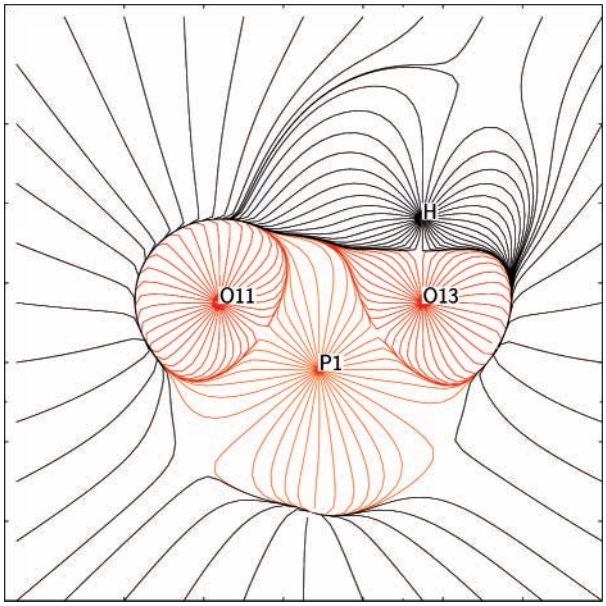

Figure 9. Experimental gradient lines of $\varphi(\mathbf{r})$ generated by the phosphate anion of the LHP (Figure 1c). The plane corresponds to O11, O13, and its hydrogen H(O13). Orange, red, and black lines stand for basins of P-, O-, and H-atoms, respectively. Ticks are set at each 1 Å.

aspartic acid. At long-range distances, the field lines start in the amino group that is situated on one side of the molecule (right side in Figure 10a) and end on the local minima associated to the lone pairs of the oxygen atoms in both carboxyl groups, one deprotonated and the other not, on the other side of the molecule (left side in Figure 10a). However, while most of the outer lines have their extrema on the aforementioned groups, at closer distances there are gradient lines ending on other parts of the molecule. In most cases, these are hydrogen atoms belonging to the inner molecular chain that exhibit finite φ-basins completely surrounded by the φ-basins of the H-nuclei of the amino group. In addition, we also find the oxygen atom belonging to the peptide bond (O1 in Figure 10b), which

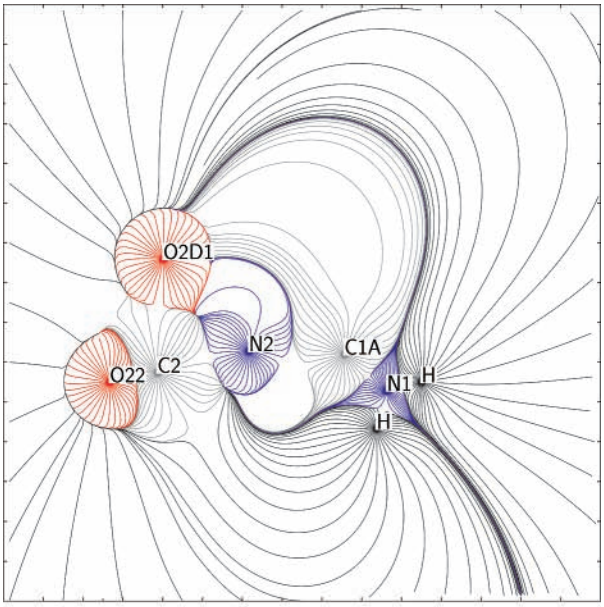

(a)

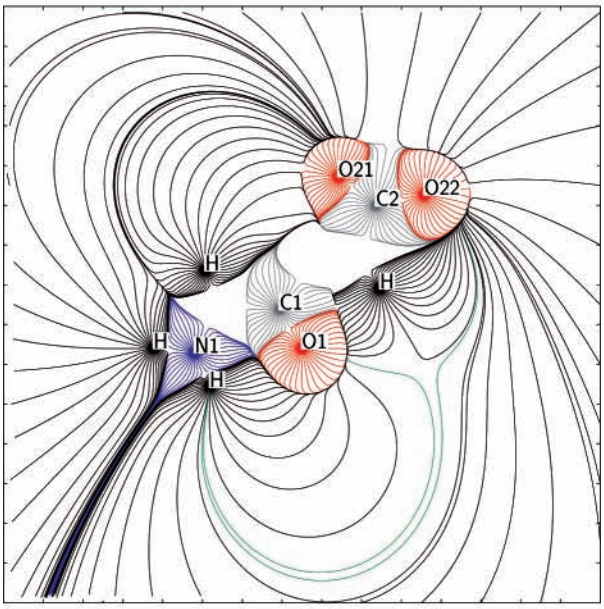

(b)

Figure 10. Experimental gradient lines of $\varphi(\mathbf{r})$ generated by the glycyl-aspartic acid (Figure 1a) in the planes defined by (a) O22, O2d1, and one H-atom bonded to N1, and (b) N1, C2, and O1. Red, blue, gray, and black lines stand for basins of O-, N-, C-, and H-atoms, respectively. In (b), both green lines are close to the border of the influence zone of the local minimum of the oxygen atom belonging to the peptide group. One of the lines is inside this influence zone, while the other is outside. Ticks are set at each 1 Å.

presents a local minimum with a finite influence zone. Thus, in Figure 10b, two primary bundles starting in two hydrogen nuclei contribute to the influence zone of this minimum. Outside the zero-flux surface delimiting this influence zone, field lines go from the amino to the carboxyl groups.

3.4. Interpretation of the Electrostatic Potential Critical Points. The relationship between zero-flux surfaces and critical points has been explored in detail for $\rho(\mathbf{r})$, and the results of this analysis can be easily applied to $\varphi(\mathbf{r})$. In the electrostatic potential, electrophilic and nucleophilic influence zones correspond to the volumes filled by the electric field lines starting and ending at the local extrema, while the zero-flux surfaces delimiting these influence zones are formed by the electric field lines starting and ending at the saddle points. Thus, every zero-flux surface has an associated saddle point, its signature depending on the type of influence zone delimited by the surface.

Some critical points of $\varphi(\mathbf{r})$ have an equivalent on $\rho(\mathbf{r})$. The most evident case corresponds to the (3, −1) critical point, i.e., a point where the scalar function exhibits a local maximum in two directions and a local minimum in the perpendicular direction. This topological point is associated to an interatomic surface delimiting an atomic basin in the case of $\rho(\mathbf{r})$, and to a zero-flux surface of $\varphi(\mathbf{r})$ delimiting a φ-basin that, as within the ρ-basin, also includes a nucleus. In both cases, the surface is defined by all the field lines starting at the (3, −1) critical point, whereas in the perpendicular direction two gradient lines come from the nuclei that are separated by the interatomic surface end at this point. For $\rho(\mathbf{r})$, these two gradient lines connecting the nuclei form the bond path that according to the AIM theory is present whenever a bonding interaction between two atoms is exhibited.[36] There is no correspondence between the bond path and the gradient lines connecting the nuclei in the $\varphi(\mathbf{r})$ topology, as (3, −1) points in the latter can be observed between pairs of atoms that do not present a bond path. Thus, in Figure 11, where both $\rho(\mathbf{r})$ and $\varphi(\mathbf{r})$ gradients are shown for the guanidinium group of the L-arginine cation in the LAP crystal structure, (3, −1) critical points of $\varphi(\mathbf{r})$, without equivalents on $\rho(\mathbf{r})$, are observed between hydrogen atoms that are connected by electric field lines. Accordingly, whereas $\varphi(\mathbf{r})$ (3, −1) points can be helpful to find the limits of the electrophilic influence zones, they are not definitively indicative of the existence of a bond path and the concomitant bonding interaction.

For $\rho(\mathbf{r})$, (3, +1) critical points (which correspond to local minima along two directions and to a local maximum along the perpendicular third direction) are associated to atomic rings. The surface associated to a critical point of this type, known as the ring surface, is formed by all of the field lines starting at the nuclei of the ring and ending at the critical point, which is also the starting point of two field lines that end either at a local minimum of $\rho(\mathbf{r})$ or go to infinity. As noticed in the topological analysis of $\rho(\mathbf{r})$ in ionic crystals,[34] ring surfaces and (3, +1) critical points play the same role for the local minima as interatomic surfaces and (3, −1) points for the nuclei. Applied to $\varphi(\mathbf{r})$, that means that (3, +1) points are associated to zero-flux surfaces limiting the nucleophilic influence zone in the same way that (3, −1) points appear on the surfaces between electrophilic influence zones.

In Figure 12a the electric field is represented for the phosphate anion of LAP. The electrostatic potential around each of the oxygen atoms that is double bonded to the phosphorus atom presents two local minima, corresponding to two lone pairs, as seen in the $\varphi(\mathbf{r})$ map of Figure 12b. Thus, a total of four local minima are observed on the border of the φ-basins that are limited by the φ-surfaces enclosing the nuclei of the double-bonded oxygen atoms. Each of these minima is therefore associated to a nucleophilic influence zone, which is separated from the adjacent ones by zero-flux surfaces that are orthogonal to the φ-surfaces enclosing the nuclei (Figure 12a).

In this way, saddle points are observed on the intersections of these orthogonal surfaces with the borders of the φ-basins that are associated to the atomic regions. The type of saddle point can be deduced by representing $\varphi(\mathbf{r})$, or its gradient, on a plane nearly tangential to the border of the φ-basin. For example, in Figure 13a, $\varphi(\mathbf{r})$ is represented on a plane near the

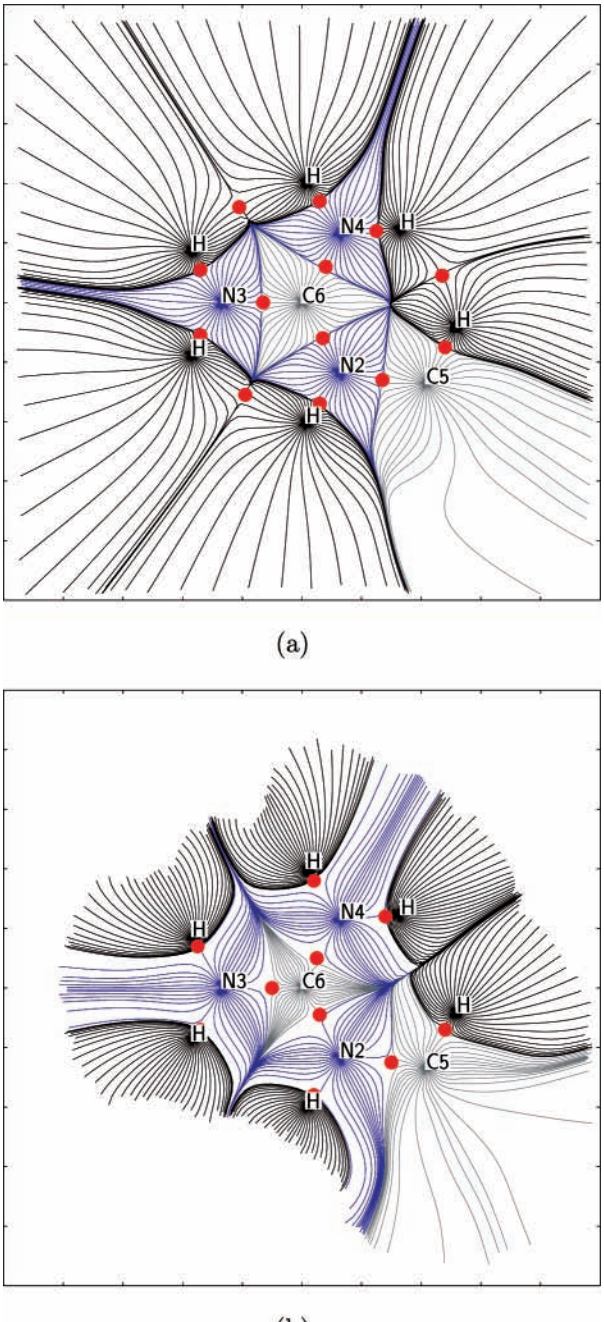

Figure 11. Experimental gradient lines of (a) $\varphi(\mathbf{r})$ and (b) $\rho(\mathbf{r})$ in the plane of the guanidinium group of the L-arginine cation in the crystal structure of LAP (Figure 1b). (3, −1) critical points are indicated by red circles. Blue, gray, and black lines stand for basins of N-, C-, and H-atoms, respectively. Ticks are set at each 1 Å.

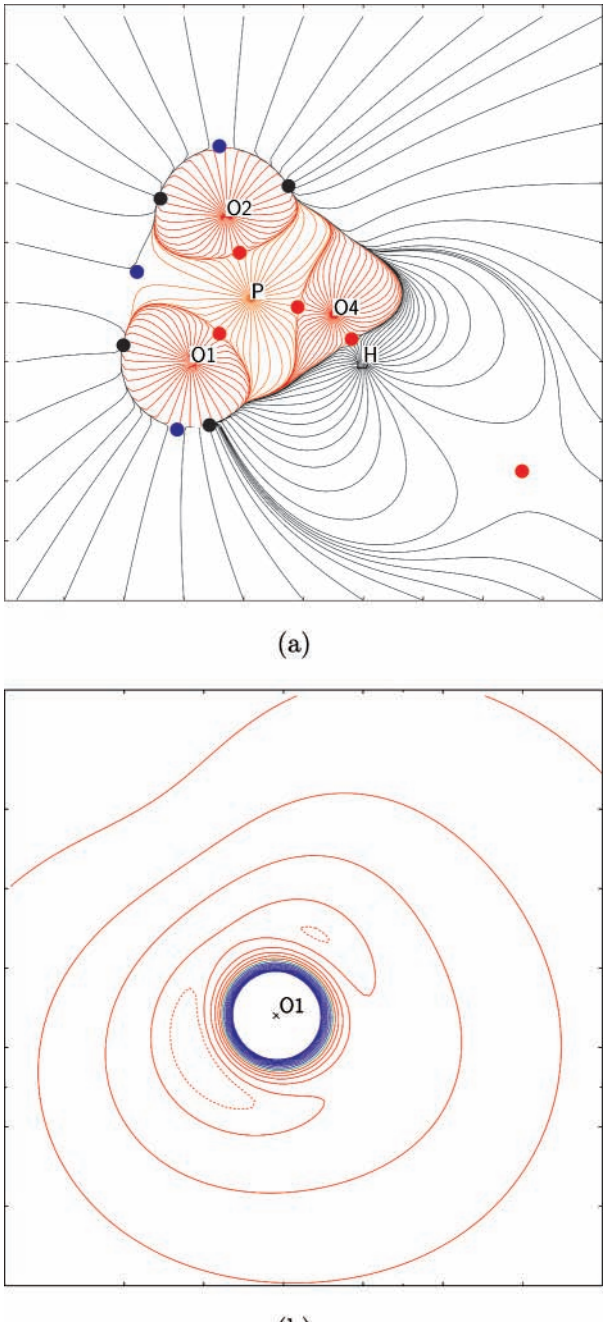

Figure 12. (a) Experimental gradient lines of $\varphi(\mathbf{r})$ generated by the phosphate anion in the crystal structure of LAP (Figure 1b). The plane is defined by O1, O2, and the H-atom bonded to O4. (3, +3), (3, −1), and (3, +1) critical points are indicated by black red, and blue circles, respectively. (b) Experimental $\varphi(\mathbf{r})$ in the plane perpendicular to the P−O1 bond, containing the O1 atom. Contours are defined as in Figure 5b, except the dashed contour that corresponds to −0.55 e Å^{-1}. Ticks are set at each 1 Å.

surface enclosing the φ-basin associated to the phosphorus nucleus and close to the φ-surfaces associated to the nuclei of the double bonded oxygens. This figure reveals that the critical point on the surface of the P-nucleus basin is of (3, +1) type, as this point is a maximum along the line joining two local minima and a minimum on the perpendicular directions. On the other side, a similar plane calculated at the critical point on the φ-surface of the hydrogen nucleus basin reveals its topological (3, −1) character, as this point appears as a maximum on the plane (Figure 13b) because it exhibits as a local minimum only along the direction perpendicular to the border of the φ-basin.

According to the topological symmetry previously observed among local maxima and local minima partitions, (3, −1) critical points in the partition carried out with local minima are analogous to (3, +1) critical points in the corresponding one with local maxima at nuclear basins. Thus, $\varphi(\mathbf{r})$ (3, −1) critical points are associated to zero-flux surfaces that are, at the same time, the border of nuclear basins and surfaces formed by a ring of local minima.

It has been seen in the previous section that the φ-basin corresponding to the hydrogen nucleus on the anion of Figure 12 determines the influence zone of the electrophilic site represented by this nucleus. As this φ-basin belongs to an anion, its influence zone must be finite. Thus, in order to interact with

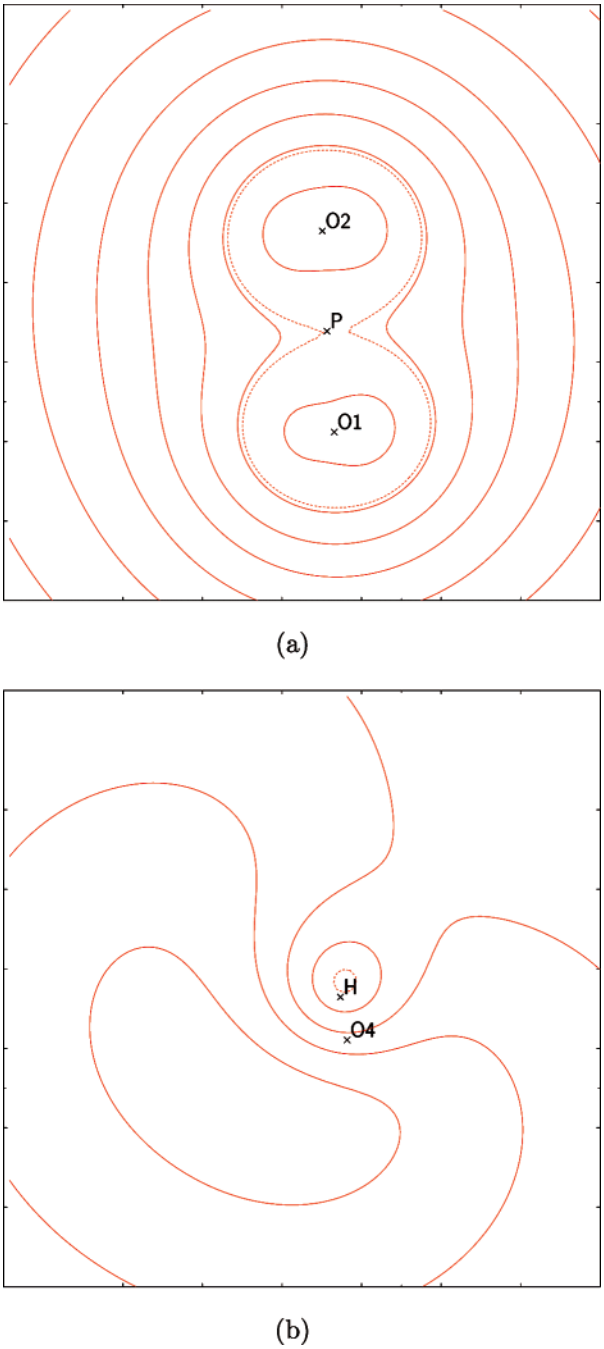

Figure 13. Experimental $\varphi(\mathbf{r})$ on the plane nearly containing the saddle critical point and approximately tangent to the surface of the φ-basin that corresponds to (a) the phosphorus region and (b) the hydrogen region represented in Figure 12. Planes are approximately tangent to the border of the φ-basin. Solid contours are set at each 0.05 e Å^{-1}, ranging (a) from −0.50 to −0.20 and (b) from −0.25 to −0.10 e Å^{-1}. The dashed contour represents the value (a) −0.457 and (b) −0.07 e Å^{-1}. Ticks are set at each 1 Å.

the electrophilic site, a negative charge coming from outside the molecule must cross the border of this region, meaning that it must overcome a potential barrier given by the value of $\varphi(\mathbf{r})$ at the point of the surface where the charge enters the influence zone. The lowest potential barrier is observed at the (3, −1) critical point, as it corresponds to the less negative value of $\varphi(\mathbf{r})$ on the surface of the influence zone. Moreover, the field line that comes from outside the molecule and ends at the (3, −1) point would be the less unfavorable trajectory for a negative charge approaching the anion, as it is along this field line that the repulsive force exerted on the approaching negative

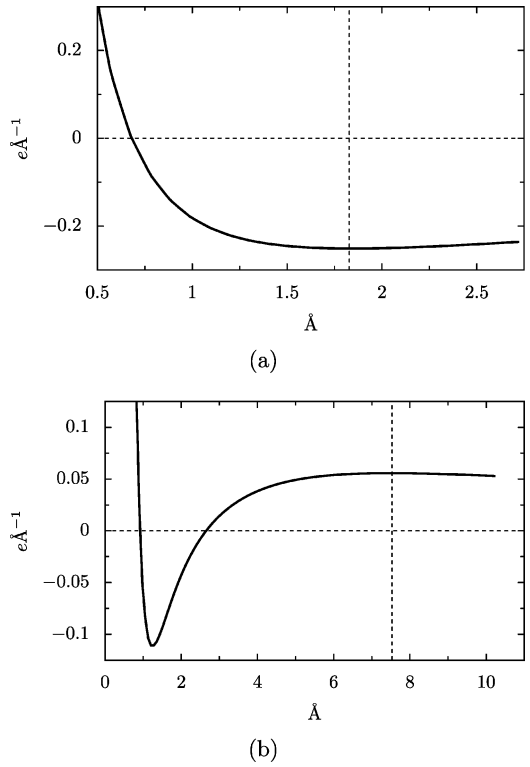

Figure 14. Experimental $\varphi(\mathbf{r})$ along the lines containing (a) the nucleus of the hydrogen atom bonded to O13 in the phosphate anion of LHP and the (3, −1) critical point, and (b) the nucleus of the oxygen atom O5 belonging to the L-arginine cation of LAP and its associated (3, +1) critical point. Both (3, −1) and (3, +1) critical points delimit the influence zones of these atoms. Ticks on the abscissas correspond to the distance from the nucleus. Vertical lines show the limit of the influence zones.

charge would be smaller. Thus, this field line shows the most favorable way for a nucleophilic attack on the electrophilic site of the anion.

The representation of the electrostatic potential along the line starting at the hydrogen nucleus and passing through the (3, −1) point in the phosphate anion of the LHP (Figure 14a) reveals the different qualitative behavior of the electric field at both sides of the zero-flux surface, pointing outward from this surface in the direction of increasing potential in both regions. It has been shown that, in the case of interanionic hydrogen bonds, the electrostatic interaction in the bonding region can be attractive in spite of the negative charge of the interacting entities,[37] a result that agrees with the existence of a finite influence zone around the hydrogen atom. Indeed, in the case of LHP, a very short hydrogen bond between phosphates is observed (d(H···O) = 1.505(5) Å, according to the neutron diffraction data[20]). This distance is shorter than that observed from the hydrogen nucleus to the (3, −1) point in Figure 14a (1.827 Å), indicating that the potential minimum that is close to the oxygen acceptor and is associated to its lone pair falls inside the influence zone of the hydrogen atom, as expected if the electrostatic interaction is attractive.

An analogous situation is observed in the case of nucleophilic groups that, belonging to cations, exhibit a finite influence zone and are therefore enclosed by zero-flux surfaces associated to (3, +1) critical points, as for the carboxyl groups in Figures 8 and 15. In Figure 15, the position of the critical point on the φ-surface, corresponding to the border of the carboxyl influence zone, is shown together with a $\varphi(\mathbf{r})$ map calculated on the environment of this point and tangent to the φ-surface. The latter map indicates that the potential is a minimum at this point of

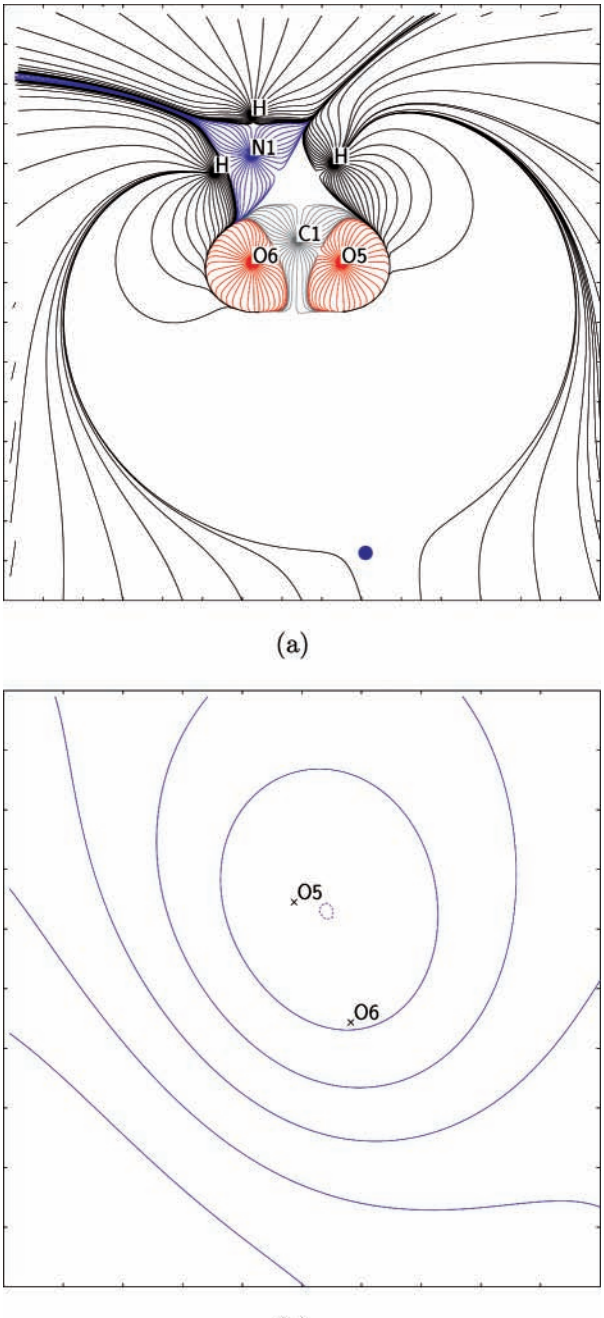

Figure 15. (a) Experimental $\varphi(\mathbf{r})$ gradient lines in the surroundings of the carboxyl group of the L-arginine cation in the crystal structure of LAP (Figure 1b). The plane is defined by O5, O6, and N1. The (3, +1) point observed on the surface of the carboxyl influence zone is identified by a blue circle. (b) Experimental $\varphi(\mathbf{r})$ on a plane nearly tangent to the surface of this influence zone and close to the (3, +1) critical point. Solid contours are set at each 0.01 e Å^{-1}, ranging from 0.05 to 0.09 e Å^{-1}. The pointed contour is at 0.041 e Å^{-1}. Both O-atoms marked in the map are 7 Å below the plane. Ticks are set at each 1 Å.

the zero-flux surface, therefore leading to its topological (3, +1) critical point character. The zero-flux surface associated to the (3, +1) point can be considered (in addition to the border of the influence zone) as the equivalent in $\varphi(\mathbf{r})$ to the ring surface on the topology of $\rho(\mathbf{r})$. Hence, the φ-ring surface is formed by the field lines generated by the nuclei that are lying on this surface. In analogy to the cases of electrophilic sites with limited influence zones, the critical point on the border of the influence zone of a nucleophilic site corresponds here to the lowest potential barrier for a positive charge approaching a nucleophilic group, and the field line starting at the (3, +1) point and going outside the molecule shows the less unfavorable trajectory for an electrophilic attack on the nucleophilic group. In Figure 15, the distances from the oxygen nuclei to the (3, +1) critical point are 7.389 and 7.835 Å, whereas in Figure 8 they are 7.037 and 7.739 Å, respectively. The similar electric field lines, φ-surfaces, and (3, +1) critical point positions observed in Figures 8 and 15 indicate the electrostatic analogy that this functional group develops in the different molecular environments represented by the singly charged cations L-argininium and L-histidinium.

As in the case of the anions, the electrostatic potential along the line containing one of the oxygen nuclei and the (3, +1) critical point shows the change of the electric field direction when comparing at both sides of the zero-flux surface (Figure 14b). Hence, a hydrogen bond involving two cations (one cation including a carboxyl group, as observed in the LAP crystal structure) would present an attractive electrostatic interaction, in spite of the positive charge of both molecules. It must be noticed that the influence zone of the carboxyl moiety is much larger than the region with negative potential associated to the oxygen lone pairs, which extends only 2.7 Å away from the oxygen nuclei.

4. Conclusions

While most of the critical points of the electron density distribution have their counterpart on the electrostatic potential topology, this last scalar field can present local minima outside the molecule that are associated to local accumulations of electrons, a feature not observed in the topology of $\rho(\mathbf{r})$. These minima give rise to a rich topology outside the molecule, involving additional saddle points and a more complex asymptotic behavior for the electrostatic potential than for the electron density.

The graphic representation of the electric field lines allows the localization of the $\varphi(\mathbf{r})$ zero-flux surfaces. In addition, it also shows the relation of this gradient vector field and the φ-surfaces with the critical points, which is helpful in the interpretation of the complex topology shown by $\varphi(\mathbf{r})$ outside the molecule. This analysis permits undertaking a partition of the space in primary bundles, which are volumes filled by electric field lines that have the same starting and ending points. The partition in φ-basins possessing the nuclei (nuclear φ-basins) can be recovered by grouping the bundles with the same origin. Alternatively, a different partition of the same space can be defined by grouping the bundles with the same end. Both partitions are only complete (i.e., they completely fill the space) in the case of neutral molecules, the partitions being incomplete in nuclear φ-basins for the anions and in local minima for the cations.

In order to provide an interpretation for each partition, the local maxima (i.e., the nuclear positions) and the local minima are assimilated to electrophilic and nucleophilic sites, respectively, with the corresponding basins indicating their influence zones. Thus, each primary bundle is the intersection of one nucleophilic influence zone and one electrophilic influence zone. As a result of its electrostatic interaction with the whole molecule, a probe-charge inside a primary bundle would be directed toward one of the extremes of this bundle, depending on its positively or negatively charged nature.

The primary bundles are delimited by zero-flux surfaces containing saddle points. The borders of the electrophilic influence zones contain (3, −1) critical points, while in the borders of the nucleophilic influence zones (3, +1) points are observed. These points correspond, respectively, to a maximum

and to a minimum of $\varphi(\mathbf{r})$ on the surface. Accordingly, they indicate the most favorable point to overcome the potential barrier before entering in the influence zone, and therefore the point where a nucleophilic or an electrophilic attack is respectively more favorable. This is of particular interest in determining which of the nucleophilic or electrophilic sites of the molecule are active at long range, as saddle points indicate where the borders of the influence zones of these sites are and, consequently, if the influence zone of a given reactive site extends without limit outside the molecule. On one hand, in the case of hydrogen bonds between either cations or anions it is clearly shown from the position of the zero-flux surfaces that the electrostatic interaction is attractive in the bonding region, in spite the overall electrostatic repulsion. On the other hand, to predict the strength of the electrostatic interaction it is necessary to determine the modulus of the electric field, which is not given by only the representation of the gradient field lines.

Acknowledgment. I.M. is grateful to Pr. Nour-Eddine Ghermani, Pr. Nouzha Bouhmaida, and Dr. Mohamed Souhassou for numerous discussions, which were very helpful for the development of the software for the calculation of the electric field lines. This work was supported by the Spanish Ministerio de Educación y Ciencia (MEC) (Project MAT2006-13572-C02-01). I.M. thanks also the MEC by a Juan de la Cierva fellowship.

References and Notes

(1) Politzer, P., Truhlar, D. G., Eds. *Chemical Applications of Atomic and Molecular Electrostatic Potentials*; Plenum Press: New York, 1981.
(2) Murray, J. S., Sen, K., Eds. *Molecular Electrostatic Potentials*; Elsevier: New York, 1996.
(3) Bader, R. F. W. *Atoms in Molecules: A Quantum Theory*; Clarendon Press: New York, 1990.
(4) Gadre, S. R.; Bendale, R. D. *Chem. Phys. Lett* **1986**, *130*, 515−521.
(5) Kumar, A.; Mohan, C. G.; Mishra, P. C. *J. Mol. Struct. (THEOCHEM)* **1996**, *361*, 135−144.
(6) Gadre, S. R.; Badane, P. K. *J. Chem. Phys.* **1997**, *1997*, 5625−5626.
(7) Politzer, P.; Parr, R. G.; Murphy, D. R. *J. Chem. Phys.* **1983**, *79*, 3859−3861.
(8) Wiener, J. J. M.; Grice, M. E.; Murray, J. S.; Politzer, P. *J. Chem. Phys.* **1996**, *104*, 5109−5111.
(9) Shuresh, C. H.; Koga, N. *J. Am. Chem. Soc.* **2002**, *124*, 1790−1797.
(10) Leboeuf, M.; Köster, A. M.; Jug, K.; Salahub, D. R. *J. Chem. Phys.* **1999**, *111*, 4893−4905.
(11) Balanarayan, P.; Gadre, S. R. *J. Chem. Phys.* **2003**, *119*, 5037−5043.
(12) Tsirelson, V. G.; Avilov, A. S.; Kulygin, A. K.; Stahn, J.; Pietsch, U.; Spence, J. C. H. *J. Phys. Chem. B* **2001**, *105*, 5068−5074.
(13) Bouhmaida, N.; Dutheil, M.; Ghermani, N. E.; Becker, P. *J. Chem. Phys.* **2002**, *116*, 6196−6204.
(14) Pathak, R. K.; Gadre, S. R. *J. Chem. Phys.* **1990**, *93*, 1770−1773.
(15) Gadre, S. R.; Shrivastava, I. H. *J. Chem. Phys.* **1991**, *94*, 4384−4390.
(16) Stewart, R. F. *Chem. Phys. Lett.* **1979**, *65*, 335−342.
(17) Coppens, P. *X-Ray Charge Densities and Chemical Bonding*; International Union of Crystallography; Oxford; Oxford University Press: New York, 1997.
(18) Pichon-Pesme, V.; Lachekar, H.; Souhassou, M.; Lecomte, C. *Acta Crystallogr., Sect. B* **2000**, *56*, 728−737.
(19) Espinosa, E.; Lecomte, C.; Molins, E.; Veintemillas, S.; Cousson, A.; Paulus, W. *Acta Crystallogr., Sect. B* **1996**, *52*, 519−534.
(20) Mata, I.; Espinosa, E.; Molins, E.; Veintemillas, S.; Maniukiewicz, W.; Lecomte, C.; Cousson, A.; Paulus, W. *Acta Crystallogr., Sect. A* **2006**, *62*, 365−378.
(21) Souhassou, M.; Espinosa, E.; Lecomte, C.; Blessing, R. H. *Acta Crystallogr., Sect. B* **1995**, *51*, 661−668.
(22) Espinosa, E.; Molins, E.; Lecomte, C. *Phys. Rev. B: Condens. Mater. Phys.* **1997**, *56*, 1820−1833.
(23) Johnson, C. K. *ORTEP-I Report ORNL-3794*; Oak Ridge Laboratory: Oak Ridge, TN, 1965.
(24) Hansen, N. K.; Coppens, P. *Acta Crystallogr., Sect. A* **1978**, *34*, 909−921.
(25) Su, Z.; Coppens, P. *Acta Crystallogr., Sect. A* **1992**, *48*, 188−197.
(26) Ghermani, N. E.; Bouhmaida, N.; Lecomte, C. *ELECTROS*; Computer Program to Calculate Electrostatic Properties from High Resolution X-ray Diffraction; CNRS UMR 7036, Université Henri Poincaré: Nancy, 1992.
(27) Souhassou, M. *NewProp*; Computer Program to Calculate the Topological Properties of Electron Density; CNRS UMR 7036, Université Henri Poincaré: Nancy, 1999.
(28) Tal, Y.; Bader, R. F. W.; Nguyen-Dang, T. T.; Anderson, S. G. *J. Chem. Phys.* **1981**, *74*, 5162−5167.
(29) Gadre, S. R.; Kulkarni, S. A.; Shrivastava, I. H. *J. Chem. Phys.* **1992**, *96*, 5253−5260.
(30) Sen, K. D.; Politzer, P. *J. Chem. Phys.* **1989**, *90*, 4370−4372.
(31) Bader, R. F. W.; Nguyen-Dang, T. T.; Tal, Y. *J. Chem. Phys.* **1979**, *70*, 4316−4329.
(32) Mata, I.; Molins, E.; Alkorta, I.; Espinosa, E. *J. Phys. Chem. A* **2007**, *111*, 6425−6433.
(33) Mohan, C. G.; Kumar, A.; Mishra, P. C. *J. Mol. Struct. (THEOCHEM)* **1995**, *332*, 171−176.
(34) Martín-Pendás, A.; Costales, A.; Luaña, V. *Phys. Rev. B: Condens. Mater. Phys.* **1997**, *55*, 4275−4284.
(35) Luaña, V.; Costales, A.; Martín-Pendás, A. *Phys. Rev. B: Condens. Mater. Phys.* **1997**, *55*, 4285−4297.
(36) Bader, R. F. W. *J. Phys. Chem. A* **1998**, *102*, 7314−7323.
(37) Braga, D.; Maini, L.; Grepioni, F.; Mota, F.; Rovira, C.; Novoa, J. *Chem. Eur. J.* **2000**, *6*, 4536−4551.